IEEE Access
Multidisciplinary ⋮ Rapid Review ⋮ Open Access Journal

Received 23 January 2024, accepted 15 February 2024, date of publication 22 February 2024, date of current version 15 March 2024.

Digital Object Identifier 10.1109/ACCESS.2024.3369030

RESEARCH ARTICLE

Nonlinear Effects in NOMA Systems Using Single Carrier Modulations: Performance Evaluation and Receiver Design

OUSSAMA BEN HAJ BELKACEM[1,2], (Member, IEEE), RUI DINIS[2], (Senior Member, IEEE), AND MOHAMED LASSAAD AMMARI[3], (Member, IEEE)

[1]Innov'Com Laboratory, Sup'Com, University of Carthage, Tunis 1054, Tunisia
[2]Instituto de Telecomunicações, Faculdade de Ciências e Tecnologia, Universidade Nova de Lisboa, 2825-515 Caparica, Portugal
[3]NOCCS Laboratory, National Engineering School of Sousse, University of Sousse, Sousse 4002, Tunisia

Corresponding author: Oussama Ben Haj Belkacem (belkacemoussema@supcom.tn)

This work was supported in part by Fundação para a Ciência e a Tecnologia (FCT) and Instituto de Telecomunicações (IT) under Project CELL-LESS6G 2022.08786.PTDC and Project UIDB/50008/2020, and in part by the Horizon Europe Marie Skłodowska-Curie Postdoctoral Fellowships HORIZON-MSCA-2022-PF-01 under Grant YAHYA-6G 101109435.

ABSTRACT Non orthogonal multiple access (NOMA) systems are very important for future communications which allows a huge increase in capacity gains when comparing to conventional orthogonal multiple access (OMA) techniques. On the other hand, the power consumption at the access point (AP) should be as low as possible, making single-carrier (SC) schemes, such as single carrier with frequency-domain equalization (SC-FDE), particularly interesting. In this paper, we consider power-efficient NOMA systems employing SC-FDE signals and present a generalized framework to characterize the signals at the output of a nonlinear device. We develop an accurate estimation of the power spectral density (PSD) of the signal associated to each user, showing that the nonlinear distortion effects on some users can be very high. Therefore, we introduce a joint iterative receiver for distortion compensation and interference cancellation based on SC-FDE characterized by low-complexity suitable for scenarios with strong nonlinear effects. Our performance results indicate that the proposed technique is able to reduce considerably the degradation associated to a high power amplifier (HPA) modeled as a memoryless polynomial and allow complexity improvements when compared to conventional schemes, especially when operating at low input back-off (IBO).

INDEX TERMS Non-orthogonal multiple access (NOMA), high-power amplifiers (HPA), single carrier with frequency-domain equalization SC-FDE, nonlinear distortion, performance evaluation.

I. INTRODUCTION

In traditional wireless communication system, multiuser design is supported through an orthogonal access, giving rise to the orthogonal multiple access (OMA) schemes. More recently, non orthogonal multiple access (NOMA) has attracted considerable interests as an alternative to OMA [1]. NOMA can generally be classified into two categories: code domain [2] and power domain [3]. Power domain NOMA multiplexing is particularly appealing due to its simplicity, since the multiple user separation is achieved through successive interference cancellation (SIC) approach [4].

For high transmission rates the multipath propagation can lead to severe time dispersion effects making recommendable the use of frequency domain equalization (FDE) techniques such as orthogonal frequency division multiplexing (OFDM) [5] and single carrier frequency domain equalization (SC-FDE) [6]. Although OFDM schemes are widely

The associate editor coordinating the review of this manuscript and approving it for publication was Walid Al-Hussaibi.

employed in broadband wireless communication systems, the transmitted signals have large envelope fluctuations, which leads to amplification difficulties. OFDM signals are also sensitive to carrier synchronization errors and deep frequency notches can lead to significant performance degradation, unless powerful error correction schemes are employed. For these reasons, SC-FDE techniques can be good alternative to OFDM schemes [7], [8], [9], [10]. Although, SC-FDE schemes can achieve acceptable performance with a simple linear FDE, the performance is substantially improved with iterative FDE schemes [7]. One of the most promising iterative FDE techniques is the IB-DFE [8] which can be regarded as a DFE where the feedforward and feedback filters are implemented in the frequency domain. Since IB-DFE techniques take into account the overall block reliability in each iteration, the error propagation effects are effectively controlled. The design of IB-DFE techniques for larger constellations and spacial multiplexing schemes have been investigated in [11]. In [12], authors have proposed an efficient transmission technique for broadcast systems where turbo IB-DFE scheme is considered with hierarchical constellations.

The combination of power domain NOMA with SC-FDE (also denoted NOMA-SC) was studied by several authors [13], [14], [15]. A new framework characterization for NOMA in hybrid massive MIMO systems employing SC-FDE transmission was proposed in [13], showing that NOMA-SC can enhance the performance of beamforming based massive MIMO systems by effectively decreasing the correlation between closely separated user channels. In [14], a frequency-domain scheduling for NOMA-SC with the assistance of iterative FDE was developed. In such scenarios like cell free technology [15], [16], SC modulation can be used in downlink transmission. Indeed, downlink communication of wireless systems typically requires a signaling scheme that allows the Access Point (AP) to use efficient power amplifiers. Under these conditions, SC-FDE techniques are a natural choice, since they allow transmitted signals with low peak-to-average power ratio (PAPR) when compared to multicarrier waveforms such as OFDM.

In practice, the system performance is affected by RF impairments, such as high-power amplifier (HPA) nonlinearity, in-phase, quadrature-phase (I/Q) imbalance [17], crosstalk and quantization errors [18]. All these imperfections are highly dependent on the transmit SC-waveform and do not show a perfectly linear behaviour. The nonlinear system behavior is often treated by utilizing a stochastic decomposition to find an equivalent linear system with uncorrelated distortion [19]

Prior works have neglected the impact of the nonlinear HPA on the system performance. The characterization of nonlinear HPA can be classified into two categories: nonlinear models with memory and memoryless models [20]. Volterra, Wiener, Hammerstein, Wiener-Hammerstein [17], are classified as memory nonlinear models. On the other hand, Solid State Power Amplifier (SSPA), Traveling Wave Tube Amplifier (TWTA), Ideal Envelope Clipping and polar memoryless nonlinearities are memoryless nonlinear models which allow polynomial approximations with relatively few terms [21]. The output of these memoryless nonlinearities can be written as a power series of the input with relatively few terms. In conventional NOMA-SC systems, the transmitted signals at the AP, corresponding to the combination of the individual signals associated to each user with the appropriate power scaling factors, are combined before the amplification process. As a result, the combined signal might have envelope fluctuations that are larger than conventional, non-NOMA SC signals, leading to in-band distortion and out-of-band radiation effects at the output signal. In this context, the effects of residual hardware impairments were studied in [22] considering a memoryless nonlinear polynomial model to characterize the HPA nonlinearities. It was shown that the outage probability (OP) performance of downlink NOMA system can be notably affected by the HPA distortions, particularly when high achievable rates are required. The error vector magnitude (EVM) is another measure that evaluates the performance degradation caused by HPA. For instance, if the desired peak-to-average power ratio (PAPR) threshold is low, this leads to an increase in the EVM, penalizing the receiver performance [23].

As far as we know, the analytical characterizing of NOMA-SC signals with nonlinear HPA and its performance evaluation has never been discussed in the literature.

In this work, we study analytically the performance of nonlinear downlink NOMA-SC signals. Based on the Bussgang decomposition [24] and the cyclostationary characteristics [25] of the NOMA-SC signal at the HPA input, we develop a theoretical approach for the statistical characterization of the transmitted nonlinear, allowing us to derive the PSD and the distribution of the residual distortion for each user.

For nonlinear NOMA-SC systems with oversampled signals, the effective part of the nonlinear distortion that affects system performance is in the in-band region of the signal. This effective distortion can be obtained by an accurate spectral characterization in the in-band region. To cope with those nonlinear distortion effects, several techniques have been proposed in literature. They can be grouped into two main categories: compensation at the transmitter [26], [27], [28] and compensation at the receiver [20], [29]. Power back-off, peak-to-average power ratio reduction techniques, and linearization techniques [26], [27] have been proposed at the transmitter. For instance predistortion techniques [28] aim to linearize the transmitter. However, some nonlinear characteristics might not possible to fully linearize, especially for systems operating close to the saturation level. In addition, the required oversampling might be too high and/or the nonlinear characteristic might not be invertable. Another issue, is the high computational complexity characterizing the predistortion techniques, a critical issue especially when

low power consumption is required. Some authors suggested performing the HPA nonlinearity compensation at the receiver. A nonlinear Bussgang receiver has been proposed to compensate the effect of the HPA nonlinearity considering NOMA-OFDM system under time-varying channels [29]. Gregorio et al. have proposed in [20] a distortion cancellation scheme improving the BER performance in OFDM-CDMA system to combat the in-band distortion.

In this work, we propose a robust NOMA-SC based on iterative FDE (Robust NOMA-IB-DFE) that takes into account the nonlinear distortion power on the computation of the MMSE equalizer parameters, as well as an enhanced distortion cancellation (DC) scheme combined with the IB-DFE receiver (Enhanced DC NOMA-IB-DFE) that jointly compensates the nonlinear HPA effects the inter-user interference components introduced by different users.

This paper is organized as follows. In Section II, we present the nonlinear downlink NOMA-SC system considered in this paper. An appropriate statistical modeling in frequency domain of the nonlinear signal is then presented in section section III. The classical and robust NOMA-IB-DFE schemes are described in section IV. In section V, we describe the proposed enhanced DC NOMA-IB-DFE receiver. A set of performance results and receiver comparison are presented and discussed in section VI. Finally, section VII concludes this work.

II. SYSTEM CHARACTERIZATION

We consider a NOMA-SC transmission where the AP equipped with single antenna is serving K single-antenna users. The time-domain block to be transmitted by the kth user has the form

$$x^{(k)}(t) = \sum_{n=-N_{cp}}^{N-1} a_n^{(k)} g\left(t - nT_s\right), \quad 1 \le k \le K, \tag{1}$$

where T_s denoting the symbol duration, N_{cp} is the appropriate cyclic prefix and $g(t)$ is the adopted pulse shape which has bandwidth above the symbol rate. $a^{(k)} = \left\{a_n^{(k)} : 0 \le n \le N-1\right\} \in \mathbb{C}^N$ is the transmitted data block, where $a_n^{(k)}$ is the nth data symbol, selected from a given constellation (e.g., a QPSK or M-QAM constellation). The sequence $a_n^{(k)}$ is a discrete-time stationary random process. Consequently, $x^{(k)}(t)$ is a continuous-time cyclostationary random process [25]. The given block is oversampled with oversampling factor N', i.e., the sampling rate is N'/T_s, leading to the time-domain transmitted block for each user $x^{(k)} = \left\{x_n^{(k)} : 0 \le n \le NN'-1\right\} \in \mathbb{C}^{NN'}$ with $x_n^{(k)} \triangleq x^{(k)}(nT_s/N')$ and $\mathbb{E}[|x_n^{(k)}|^2] = 2\sigma_x^2$. Based on NOMA scheme, the time domain combined signal, i.e., $x = \left\{x_n : 0 \le n \le NN'-1\right\} \in \mathbb{C}^{NN'}$, can be expressed as

$$x = \sum_{k=1}^{(k)} \xi^{(k)} x^{(k)}, \tag{2}$$

with $\xi^{(k)}$ denoting the power allocation coefficient for each user, with $\xi^1 \ge \cdots \ge \xi^{(k)}$. The power separation ratio (PSR) between users k and $k-1$ is given by [30]

$$\beta = 20\log_{10}\left(\frac{\xi^{(k)}}{\xi^{(k+1)}}\right). \tag{3}$$

To model the HPA component, we consider the bandpass memoryless nonlinearity characterized by the amplitude-to-amplitude (AM/AM) and the amplitude-to-phase (AM/PM) conversion functions [31]. If the oversampling factor is large enough to make aliasing effects at the nonlinearity out negligible, we can study nonlinear effects on the sampled signals. Thus, the signal at the HPA input by can be expressed as

$$x_n = r_n \exp(j\theta_n), \tag{4}$$

where $r = \left\{|x_n| : 0 \le n \le NN'-1\right\} \in \mathbb{C}^{NN'}$ and θ_n is the input phase of x_n. Then the signal at the output of the memoryless nonlinear HPA can be expressed as

$$\begin{aligned} z_n &= f(r_l)\exp(j\theta_l) \\ &= A(r_n)\exp\left(jB\left(r_n\right)\right)\exp\left(j\theta_n\right)), \end{aligned} \tag{5}$$

where $f(r_n) = A\left(r_n\right)\exp\left(jB\left(r_n\right)\right)$ with $A(.)$ and $B(.)$ denote the HPA (AM/AM) and (AM/PM) conversion functions, respectively. In this work, we are interested in the polar polynomial model that can be expanded as a power series on r_n [32].

$$f(r_n) = \sum_{i=0}^{\infty} \eta_{2i+1} r_n^{2i+1}, \tag{6}$$

In practice, it is usual to use a polynomial with just a few terms as an approximation. The number of terms needed to characterize a given nonlinearity is usually low and depends on the values of r_n. The nonlinear coefficients η_{2i+1} are in general complex numbers. In the strictly memoryless case with real value coefficients, only the AM/AM conversion is taken into account. We note that only odd-order product terms are considered in (6) due to the fact that the signals generated from the even order terms are outside the frequency band of interest. In this paper, the HPA coefficients are assumed to be known, to simplify the analysis.The operating point of the amplifier is usually identified by the input back-off (IBO) defined as

$$IBO = 10\log_{10}\left(\frac{A_{sat}^2}{2\sigma_x^2}\right), \tag{7}$$

where A_{sat} is the HPA input saturation level.

III. THEORETICAL ANALYSIS OF THE RESIDUAL NONLINEAR DISTORTIONS

Let us consider the SC signal presented in (1). The HPA input is the overall NOMA signal given by

$$x(t) = \sum_{k=1}^{(k)} \sum_{n=-CP}^{N-1} \xi^{(k)} a_n^{(k)} g\left(t - nT_s\right), \quad 1 \le k \le K \tag{8}$$

We can easily show that the combined signal $x(t)$ is cyclostationary and the cyclic autocorrelation function $R_{xx}(t,\tau) = \mathbb{E}[x(t-\tau)x^*(t)]$ is periodic in t, with period T_s. In nonlinear SC transmission, the distribution of $x(t)$ is not easy to compute and, in general, does not belong to a know family. This makes it very difficult to analytically derive the impact of a nonlinearities on the symbols. To overcome this issue, we take advantage of the input signal characteristic and the generalized Bussgang's theorem [24] to approximate the nonlinear output signal. The Bussgang's theorem states that, for a nonlinearity with cyclostationnary process, the crosscorrelation between the oversampled input signal and the signal at the nonlinearity output is proportional to the cyclic autocorrelation function of the input signal, i.e., $R_{xz}(t,\tau) = \alpha(t)R_{xx}(t,\tau)$ where $R_{xz}(t,\tau) = \mathbb{E}[|x(t-\tau)z^*(t)]$. $\alpha(t)$ is a scale factor given by

$$\alpha(t) = \frac{\mathbb{E}[x(t)z^*(t)]}{\mathbb{E}[z(t)z^*(t)]} \tag{9}$$

We note that since the input signal of the HPA is cyclostationary with the period T_s/N' the output signal of the amplifier is also cyclostationary with the same period [33], and thus

$$\alpha(t) = \alpha(t + nT_s/N') \tag{10}$$

Consequently, for the NOMA transmission scheme the relationship between the baseband equivalent input and output HPA signal for the kth user can be written as

$$z_n^{(k)} = z_n = \underbrace{\alpha\xi^{(k)}x_n^{(k)}}_{\text{Useful signal}} + \underbrace{\underbrace{\alpha\sum_{u\neq k}^{(k)}\xi^{(k)}x_n^{(k)}}_{\text{IUI}} + \underbrace{d}_{\text{NL-noise}}}_{\text{Equivalent-noise}}, \tag{11}$$

where $d = \{d_n : 0 \le n \le NN' - 1\} \in \mathbb{C}^{NN'}$ is the nonlinear noise that is assumed to be uncorrelated with input signal. From (11), the transmitted data to the kth includes its desired signal and the equivalent noise caused by the interference from other users and the HPA component. In general, the kth user considers only the linear instantaneous term in the detection procedure. It is clear that the equivalent noise has a significant impact for the low power users. Indeed, the nonlinear noise (NL-noise) term is constant for different k users. However, the magnitude of the inter-user interference (IUI) term is very high compared to useful power of the devices that are closer to the AP. Since the users data symbols are assumed to be statistically independent and still making use of the Bussgang's decomposition, the cyclic autocorrolation function relative to the HPA output can be expressed as [34]

$$R_z(t,\tau) = \mathbb{E}[|z(t-\tau)z^*(t)] = |\alpha\xi^{(k)}|^2R_x(t,\tau) + \alpha^2\sum_{u\neq k}^{(k)}|\xi^u|^2R_x(t,\tau) + R_d(t,\tau), \tag{12}$$

with $R_d(t,\tau)$ denoting the cyclic autocorrolation function of the nonlinear distortion. Considering the last decomposition, and using the fact that the input signal is uncorrelated with the distortion component in frequency domain,[1] the PSD of the clipped NOMA-SC signal is given by

$$G_{z^{(k)}}(f) = |\alpha\xi^{(k)}|^2G_x(f) + G_{\omega^{(k)}}(f), \tag{13}$$

with $G_x(f) = \text{DFT}(R_x(t,\tau))$ and $G_{z^{(k)}}(f)$ represents the PSD of the residual noise for each user k, given by

$$G_{\omega^{(k)}}(f) = |\alpha|^2\sum_{u\neq k}^{(k)}|\xi^{(u)}|^2G_x(f) + G_d(f), \tag{14}$$

where $G_d(f) = \text{DFT}(R_d(t,\tau))$.

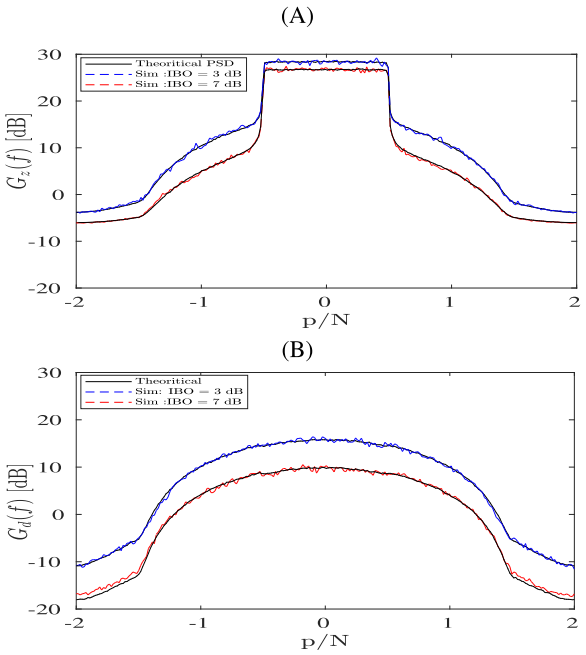

FIGURE 1. Theoretical and simulated PSDs of the clipped NOMA-SC signal (A) and of the distortion component (B) considering different values of IBO with $N = 256$ and $O = 4$.

Fig. 1, shows the theoretical and simulated PSDs of the nonlinearly NOMA distorted signal $G_z(f)$ and of the distortion component $G_d(f)$ for $K = 2$, $k = \{1, 2\}$. It should be noted that our analysis can be easily extended to a higher number of users K. For these results we assume $N = 256$, an oversampling factor[2] $N' = 4$ and 3-order polynomial HPA model. The nonlinear amplifier is set to operate at IBOs of 3 dB and 7 dB. It should be noted that the theoretical results are obtained through the Bussgang approximation expressed in (13). Clearly, the theoretical PSDs $G_z(f)$ and $G_d(f)$ match with the simulated PSDs for different values of IBOs with a high degree of accuracy. It is worth noticing that when the IBO decreases, the performance gaps becomes

[1]The DFT block acts as a block which transforms a set of independent complex random variables to a set of independent complex random variables and the same applies to their sum. This conjecture can be experimentally verified by simulation.

[2]Since we are mainly concerned with the in-band region, an oversampling factor of 4 is assumed to avoid aliasing effects.

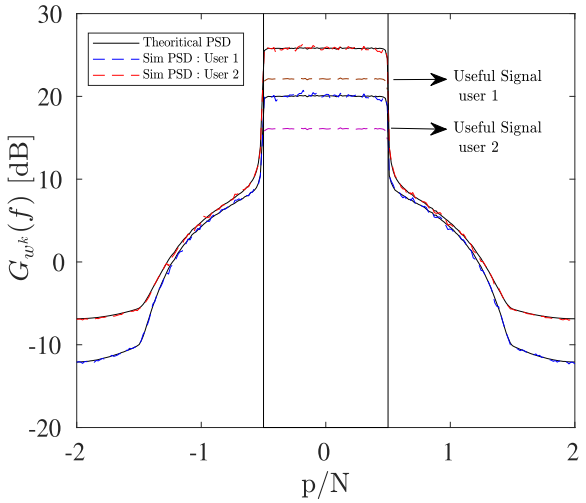

FIGURE 2. Comparison of the PSD of the equivalent noise $w^{(k)}$ component and useful signal, with $N = 256$, $O = 4$ and IBO = 7 dB.

more pronounced. Moreover, using an oversampling factor of M > 1, the power of the quantization noise will be distributed over a bandwidth larger than that of the received signal. In this case, that part of quantization noise can be filtered out by the detection filter and will not degrade the system's performance.

To evaluate the impact of linearity for each user, Fig. 2 depicts the theoretical and simulated PSDs of the equivalent distortion component $\omega^{(k)}$ for low and high power users. We can observe that the analytical results based on Bussgang approximation and simulations match well. Moreover, we can note that for the low power users (i.e., the user with index $k = 2$), the magnitude of the effective distortion signal, can be even stronger than the useful signal. This means that the performance will be more conditioned on the nonlinear distortion effects especially for strong nonlinearities (i.e, low IBO values) and considering the high power user (i.e., the user with index $k = 1$).

IV. ROBUST NOMA-IB-FDE

Block-based SC waveforms usually employ linear FDE techniques to overcome the effects of a multipath channel. However, the performance is much better if the linear FDE is replaced by a nonlinear equalizer, and the IB-DFE is one of the most promising nonlinear FDE approaches, with excellent performance/complexity tradeoffs. In the NOMA case, the IB-DFE should be designed not only to tackle ISI, but also to reduce the inter-user interference (IUI). Although the IB-DFE complexity increases with the number of equalization iterations, it typically converges to a steady-state behaviour after just about 3 to 5 iterations [35].

In this section we design an IB-DFE receiver for nonlinear NOMA signals that is based on the Bussgang approximation. The oversampled transmitted blocks for each user k, $z^{(k)} = \left\{z_n^{(k)} : 0 \le n \le NN' - 1\right\} \in \mathbb{C}^{NN'}$, are passed to the frequency domain, leading to the nonlinear blocks $Y^{(k)} = \left\{Y_p^{(k)} : 0 \le p \le NN' - 1\right\} \in \mathbb{C}^{NN'}$. If the cyclic prefix is longer than the overall channel impulse response length then

$$\begin{aligned} Y_p^{(k)} &= H_p^{(k)} Z_p^{(k)} + N_p^{(k)} \\ &= H_p^{(k)} \left(\alpha \xi^{(k)} X_p^{(k)} + \alpha \underbrace{\sum_{u=1}^{k-1} \xi^{(u)} X_p^{(u)}}_{\text{SIC}} \right. \\ &\quad \left. + \alpha \underbrace{\sum_{v=k+1}^{(k)} \xi^{(v)} X_p^{(v)}}_{\text{IUI}} + D_p \right) + N_p^{(k)} \end{aligned} \tag{15}$$

where $Z^{(k)} = \left\{Z_p^{(k)} : 0 \le p \le NN' - 1\right\} \in \mathbb{C}^{NN'}$ denotes the DFT($z^{(k)}$), $D = \left\{D_p : 0 \le p \le NN' - 1\right\} \in \mathbb{C}^{NN'}$ is the DFT($\mathbf{d}$) and $H^{(k)} = \left\{H_p^{(k)} : 0 \le p \le NN' - 1\right\} \in \mathbb{C}^{NN'}$ represents the overall channel frequency response for the pth subcarrier corresponding to user k. $N^{(k)} = \left\{N_p^{(k)} : 0 \le p \le NN' - 1\right\} \in \mathbb{C}^{NN'}$ is the additive white Gaussian noise (AWGN) terms in the frequency-domain, including the inter-cell interference, which can be assumed as an additional noise term that could be absorbed the noise power spectral density [36]. These noise samples are complex Gaussian with zero mean and variance $2\sigma^2_{N^{(k)}}$, i.e, $N^{(k)} \sim CN(0, 2\sigma^2_{N^{(k)}})$.

It should be also noted that, although the nonlinear input samples $x_n^{(k)}$ are not Gaussian, the distortions samples d are approximately Gaussian. Consequently, the distortions signal can be modelled by $d \sim CN(0, 2\sigma_d^2)$ and $D \sim CN(0, 2\sigma_D^2)$. The accuracy of this Gaussian approximation is shown in Fig. 3.

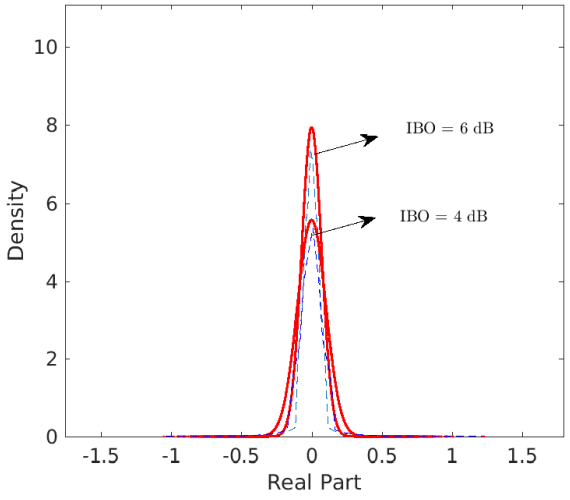

FIGURE 3. Distribution of the real part of the distortion signal d with different value of IBO.

According to the power domain NOMA scheme, the kth user decodes the signals of the high power users ($u < k$) and removes the message before detecting the corresponding signals (i.e., employing a successive interference cancellation (SIC) approach), while users with lower power (i.e., for $v > k$), the IUI in (15)) will be treated as a noise component. Clearly, from previous equation, the impact of a time-dispersive channel reduces to a scaling factor for each frequency.

Generally, a linear FDE equalization is often used in conjunction with SC modulation to reduce the ISI caused by the multipath channels and IUI levels. However, a non-linear FDE receiver, based on feedword and feedback equalization, can achieve better this goal leading to the so-called "IB-DFE with hard decision" [8]. Under this condition, the estimated frequency-domain samples $\tilde{X}^{(k)} = \left\{\tilde{X}_p^{(k)} : 0 \le p \le NN' - 1\right\} \in \mathbb{C}^{NN'}$, associated with the kth user for the lth iteration, are given by

$$\tilde{X}_p^{(k,l)} = F_p^{(l)}\left(Y_p^{(k)} - \alpha H_p^{(k)} \sum_{u=1}^{k-1} \xi^{(u)} X_p^{(u,l)}\right) - B_p^{(k,l)} \hat{X}_p^{(k,l-1)} \tag{16}$$

The equalized signal represented in (16)can be decomposed as the sum an useful signal and an approximately Gaussian distributed noise component given by

$$\tilde{X}_p^{(k,l)} \approx \alpha \xi^{(k)} X_p^{(k,l)} + \Omega_p^{(k,l)} - B_p^{(k,l)} \hat{X}_p^{(k,l-1)}, \tag{17}$$

with $\Omega_p^{(k,l)}$ denotes the residual noise from the lth FDE iteration defined as

$$\Omega_p^{(k,l)} = \alpha \underbrace{\sum_{v=k+1}^{(k)} \xi^{(v)} \tilde{X}_p^{(v,l)} + D_p^{(l)}}_{\text{IUI}} + F_p^{(l)} N_p^{(k,l)}, \tag{18}$$

where $\left\{F_p^{(k,l)}, B_p^{(k,l)} : 0 \le p \le NN' - 1\right\} \in \mathbb{C}^{NN'}$ denote the feedforward and the feedback coefficients, respectively. For the conventional MMSE technique [37], the optimum coefficients $F_p^{(k,l)}$ and $B_p^{(k,l)}$ maximizing the overall SNR are defined by [9]

$$F_p^{(k,l)} = \frac{\kappa^{(k,l)} \left(H_p^{(k)}\right)^*}{\left[\left(1 - (\rho^{(l-1)})^2\right) \left|H_p^{(k)}\right|^2 + \Psi_p^{(k)}\right]}, \tag{19}$$

and

$$B_p^{(k,l)} = \rho^{(l-1)} \left(F_p^{(k,l)} H_p^{(k)} - 1\right), \tag{20}$$

where $\Psi_p^{(k)}$ is composed with the noise-and-nonlinear distortion-to-signal ratio levels associated to the pth subcarrier and the kth user, defined as

$$\Psi_p^{(k)} = \frac{2\sigma_{N^{(k)}}^2 + G_d(p)}{2\sigma_X^2}, \tag{21}$$

and $\kappa^{(k,l)}$ is a normalizing factor to ensure

$$\frac{\sum_{p=1}^{NN'-1} F_p^{(k,l)} H_p^{(k)}}{NN'} = 1 \tag{22}$$

$\left\{\hat{X}_p^{(k,l)}, : 0 \le p \le NN' - 1\right\} \in \mathbb{C}^{NN'}$ represents the hard-decisions for a given iteration l. As shown in [11], the hard-decisions can be written as the sum of two uncorrelated components, i.e.,

$$\hat{X}_p^{(k,l)} \approx \rho^{(k,l)} X_p^{(k,l)} + \Delta_p^{(k,l)}, \tag{23}$$

where $\rho^{(k,l)}$ concerns the blockwise reliability of the decisions used in the feedback loop from the lth iteration, defined as

$$\rho^{(k,l)} = \frac{E[\hat{x}^{(k,l)}(x^{(k)})^*]}{E[(x^{(k)})^*]}. \tag{24}$$

The term $\Delta_p^{(k,l)}$ represents an error term relatively to the transmitted symbols for each kth user, given by

$$E[|\Delta_p^{(k,l)}|] = 2\left(1 - |\rho^{(k,l)}|^2\right)\sigma_X^2. \tag{25}$$

Clearly, according to (19 and 21), the conventional receiver (i.e., using the conventional MMSE equalizer) does not take into account the residual distortion after each iteration. Indeed, based on (18), the IB-DFE consider the distortion levels as a IUI. By taking advantage of (24), the residual distortion power after the lth iteration can expressed as

$$\sigma_{D_p^{(l)}} = \frac{1}{2}\left(1 - |\rho^{(k,l)}|^2\right) G_d(p) \tag{26}$$

consequently, The feedforward equalizer associated to that robust MMSE receiver is defined as

$$F_p^{(k,l)} = \frac{\kappa^{(k,l)} \left(H_p^{(k)}\right)^*}{\left[\left(1 - (\rho^{(l-1)})^2\right) \left|H_p^{(k)}\right|^2 + \Psi_p^{(k,l)}\right]}, \tag{27}$$

where $\Psi_p^{(k,l)}$ corresponds to the noise-and-residual nonlinear distortion-to-signal ratio levels associated to the pth subcarrier and the kth user for each iteration, given by

$$\Psi_p^{(k,l)} = \frac{2\sigma_{N^{(k)}}^2 + G_{d^{(k)}}(p)(1 - |\rho^{(k,l)}|^2)}{2\sigma_X^2}, \tag{28}$$

Nevertheless, the Robust NOMA-IB-DFE design, is not able to compensate totally the nonlinear noise caused by the HPA (i.e., only the IUI and ISI levels are reduced through the feedback equalization. Under these conditions, the system performance will be degraded resulting a high error floor, especially, for low power users when considering a low IBO values, even when β is high.

Throughout this work, we refer to the target user by 'high/low power user' and the signal detection for each user by 'high/low power signal'. Fig. 4 and Fig. 5 show the BER associated to both the high power and low power signals from the perspective of the low power user, considering

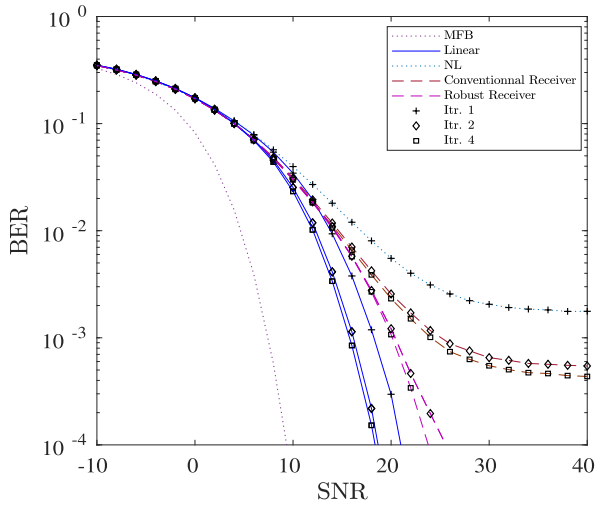

FIGURE 4. Conventional Vs. Robust NOMA-IB-DFE receivers performance of high-power signals from the perspective of the low-power user with IBO = 6 dB.

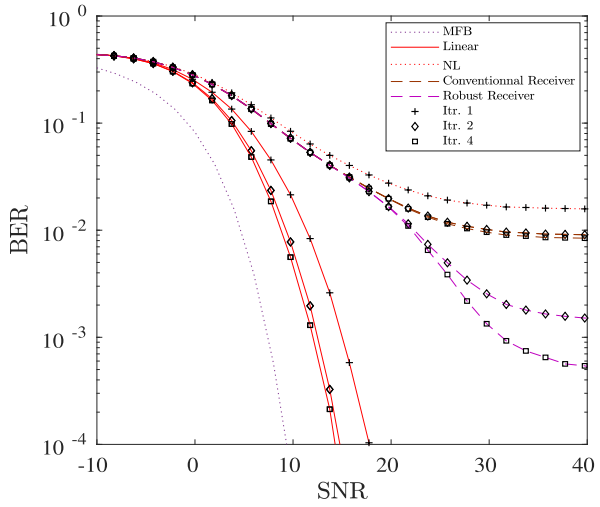

FIGURE 5. Conventional Vs. Robust NOMA-IB-DFE receivers performance of low-power signals from the perspective of the low-power user with IBO = 6 dB.

Conventional and Robust NOMA-IB-DFE scenarios with $\beta = 9$ dB and IBO $= 6$ dB. The number of iterations is $I = 4$. To make the figures more clear, the BER performances presented in this work only show iterations 1, 2 and 4, since the 3rd iteration does not add relevant detail regarding $Itr = 4$. Moreover, the first iteration (i.e., $Itr = 1$) characterized the same nonlinear behavior for all proposed receiver since the initialized parameter $|\rho^{(k,1)}|^2) = 0$. From these figures, it can be observed that, regardless of the HPA component, the Robust receiver presents significant performance gains compared to the Conventional IB-DFE receiver, especially, for the detection for the high power signal. Therefore, in presence of nonlinear distortion effects, the Robust NOMA-IB-DFE receiver should be considered. However, it can be noted from Fig. 5 that although we used the Robust NOMA-IB-DFE, the residual distortion reduced considerably the detection performance and decreases the BER especially for the detection of the low power signal. Indeed, for this scenario, the nonlinear degradation is conditioned by the distribution of the joint NOMA signals (i.e., it is mainly conditioned by the high-power signals), which is very large comparing to the useful part of the low-power user, so it cannot be ignored by the receiver.

V. ENHANCED DC-NOMA-IB-FDE DESIGN

As mentioned before, the main issue of the Robust NOMA-IB-DFE, based on the Bussgang approximation, is that this technique cannot cancel perfectly the nonlinear distortion effects, which can lead to significant performance degradation. In this section, we present an enhanced iterative distortion cancellation (DC) called Enhanced DC-NOMA-IB-DFE receiver, to combat the in-band degradation by reducing, jointly, the residual distortion component and the IUI for each user. Fig. 6 shows the block diagram of the proposed receiver for the low-power user (i.e., $k = 2$). Essentially, from each user k, the nonlinear distortion term D_p should be estimated from the high-power signal and canceled from the received data to detect its own signal.

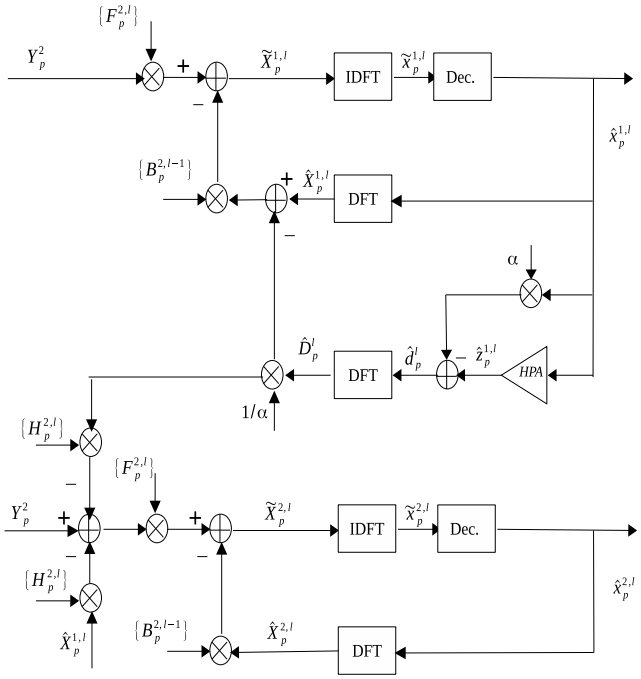

FIGURE 6. Enhanced iterative DC-NOMA-IB-DFE design for the detection of high power and low power signals from the perspective of the low power user.

Let us start by describing the detection of the high power signal considering the user k. Using the recovered symbols $\tilde{X}_p^{(1,l)}$, corresponding to the high power signal, the time domain data at the lth iteration is reproduced via IDFT, i.e., $\tilde{x}_n^{(1,l)} = \text{IDFT}\left(\tilde{X}_p^{(1,l)}\right)$, where $\left\{\tilde{x}_n^{(1,l)}, : 0 \leq n \leq NN' - 1\right\} \in \mathbb{C}^{NN'}$. Assuming perfect estimation of nonlinear memoryless coefficients (a reasonable assumption, since the

nonlinear parameters change very slowly compared to channel variations), the estimated distortion signal $\hat{d}^l = \left\{d_n^l : 0 \leq n \leq NN' - 1\right\} \in \mathbb{C}^{NN'}$, is obtaining by submitting the estimated high power signal $\hat{x}_n^{(1,l)}$, from the amplified symbol $\hat{z}^{(1,l)}) = \left\{z_n^{(1,l)} : 0 \leq n \leq NN' - 1\right\} \in \mathbb{C}^{NN'}$, expressed as

$$\hat{d}_n^{(l)} = \left(\sum_{i=0}^{\infty} \eta_{2i+1} (\hat{r}_n^{(1,l)})^{2i+1} \exp(j\hat{\theta}_n^{(1,l)})\right) - \alpha(\hat{x}_n^{(1,l)}) \quad (29)$$

with $\hat{r}_n^{(1,l)}$ and $\hat{\theta}_n^{(1,l)}$ denoting the absolute value and the phase estimates of $\hat{x}_n^{(1,l)}$. Applying the DFT operator, the signal for detection for the high power signal purposes at the lth iteration, from which we jointly cancel the distortion at the $(l-1)$th iteration, can be obtained as follows

$$\begin{aligned}\tilde{X}_p^{(1,l)} &= F_{p,equ}^{(k,l)}\left(Y_p^{(k)} - H_p^{(k)}\frac{\hat{D}_p^{(l-1)}}{\alpha}\right) - B_{p,equ}^{(1,l)}\hat{X}_p^{(1,l-1)} \\ &\simeq \left(\xi^1 \hat{X}_p^{(1,l)} + \sum_{v=2}^{(k)} \xi^{(v)} \tilde{X}_p^{(v,l)} + \frac{D_p - \hat{D}_p^{(l-1)}}{\alpha} \right. \\ &\quad \left. + F_p^{(k,l)} N_p^{(k)}\right) - B_p^{(1,l)}\hat{X}_p^{(1,l-1)}, \end{aligned} \quad (30)$$

Consequently, and doing a successive user cancellation, the signal detection corresponding to the kth user at the iteration l can be expressed as

$$\begin{aligned}\tilde{X}_p^{(k,l)} = F_{p,equ}^{(k,l)}\left(Y_p^{(k)} - H_p^{(k)}\sum_{u=1}^{(k-1)} \xi^{(u)}\hat{X}_p^{(u,l)} \right. \\ \left. - H_p^{(k)}\frac{\hat{D}_p^{(l-1)}}{\alpha}\right) - B_{p,equ}^{(k,l)}\hat{X}_p^{(k,l-1)}, \end{aligned} \quad (31)$$

where $F_{p,equ}^{(k,l)}$ and $B_{p,equ}^{(k,l)}$ represent the feedforward and feedback coefficients associated to the MMSE receiver taking into account the distortion compensation at the lth iteration, given by

$$F_{p,equ}^{(k,l)} = \frac{\kappa^{(k,l)}\left(H_p^{(k)}\right)^*}{\left[\left(1 - (\rho^{(l-1)})^2\right)\left|H_p^{(k)}\right|^2 + \Psi_{p,equ}^{(k,l-1)}\right]}, \quad (32)$$

and

$$B_{p,equ}^{(k,l)} = \rho^{(l-1)}\left(F_{p,equ}^{(k,l-1)}H_p^{(k)} - 1\right), \quad (33)$$

with $\Psi_{p,equ}^{(k,l)}$ denoting the equivalent distortion and noise to signal ratio levels, when using a iterative distortion cancellation, i.e.,

$$\Psi_{p,equ}^{(k,l)} = \frac{2\sigma^2_{\hat{D}_{p,equ}^{(l)}}(1 - |\rho^{(k,l)}|^2) + 2\sigma^2_{N^{(k)}}}{2\sigma_X^2} \quad (34)$$

where $\sigma^2_{\hat{D}_{p,equ}^{(l)}} = \frac{1}{2}\left(G_d^{(l)}(p) - 2\sigma^2_{\hat{D}^{(l)}}\right)$. Taking advantage of (26), we can write we can write

$$\sigma^2_{\hat{D}_{p,equ}^{(l)}} = \frac{1}{2}\left(1 - |\rho^{(k,l)}|^2\right)\left(G_{d^{(l)}}(p) - G_{\hat{d}^{(l)}}(p)\right) \quad (35)$$

Although (23) and (25) may be considered coarse approximations, they allow a simple computation of $\left(G_{d^{(l)}}(p) - G_{\hat{d}^{(l)}}(p)\right)$. Thus, we obtain, after some straightforward manipulation, the following expression

$$\sigma^2_{\hat{D}_{p,equ}^{(l)}} \approx (1 - |\rho^{(k,l)}|^2)^2\sigma_X^2 \quad (36)$$

We note that we need to have $\rho^{(k,l)} \approx 1$ to assure accurate estimation of $\sigma^2_{\hat{D}_{p,equ}^{(l)}}$. Naturally, the first iteration represents the detection using the conventional NOMA-IB-DFE and Robust NOMA-IB-DFE (i.e, considering the nonlinear effects). Doing this, we create a good synergy between user's interference minimization and distortion compensation. Indeed, the proposed detection scheme, takes advantage of it by updating the MMSE equalizer for each iteration considering the estimated distortion level.

It should be noted that, one of the advantages of the Enhanced DC-NOMA-IB-DFE is its moderate computational complexity, which does not preclude an excellent capability for removing nonlinear distortion, as will be shown in the next section. Indeed, the additional complexity measured in terms of the number of FFT/IFFT operations, distortion detection and cancellation operations as well as the computation charge required for the calculation of the feedforward and feedback coefficients, are negligible compared to the Robust NOMA-IB-DFE receiver. Moreover, the additional operations have low computational complexity when compared with that of the other required operations at the receiver side such as synchronization, channel estimation, channel decoding, etc. Therefore, the overall computing burden of the Enhanced NOMA-DC-IB-DFE is similar to conventional techniques.

Table 1 shows the computational complexity of the Enhanced NOMA-DC-IB-DFE compared to the predistortion NOMA-IB-DFE approach described in [29] and [38], based on the well-known multi-layer perceptron (MLP) neural network (NN) model. Since the IB-DFE is performed in the same way in both techniques, its corresponding computational complexity is not taken into account here. Only the distortion compensation methods will be evaluated in term of complexity. For the predistortion NOMA approach of [38] the authors used a feed-forward MLP with two inputs, two outputs and one hidden layer with three neurons noted ϑ, ι and κ, respectively. It is worth to mention that the complexity of neural network training step is not considered in our complexity study because it is realized in the off-line step and only the complexity required to run the neural network predistorter is considered. To process a SC frequency-domain NN' samples, the computational complexity of the predistortion NOMA is estimated as $2 \times I_{\max} \times \mathcal{O}(NN'[\vartheta\iota + \iota\kappa + \kappa])$ [29]. The DC technique proposed in our receiver needs two NN'-point FFT/IFFT operations to be implemented for each iteration. Consequently, the required operation number relative to our proposed method, is estimated as $2 \times I_{\max} \times \mathcal{O}(NN' \log NN')$. Based on the

result shown in Table 1, the complexity of the Enhanced DC NOMA-IB-DFE receiver is always lower than that of the predistortion approach. It is worth noting that for a large number of subcarriers, the computational gain of the predistortion approach over the proposed Enhanced DC NOMA-IB-DFE receiver decrease. This is due to the low computational complexity related to the trained NN model when compared with the NN' point FFT/IFFT. For instance, most SC systems employ a moderate number of subcarriers (e.g., 128, 256, 512), thus, the advantages of the proposed receiver are clear.

VI. PERFORMANCE RESULTS

In this section we present a set of performance results concerning SC-IB-DFE receivers in NOMA context under frequency selective channels with uncorrelated Rayleigh fading. We consider blocks with $N = 256$ QPSK/16 QAM symbols[3] plus an appropriate cyclic prefix. We also assume perfect synchronization and the adopted nonlinear characteristic are modeled by 3-order polynomial HPA model. The BER performance associated to the MFB and the linear NOMA-IB-DFE are plotted for the sake of performance comparisons.

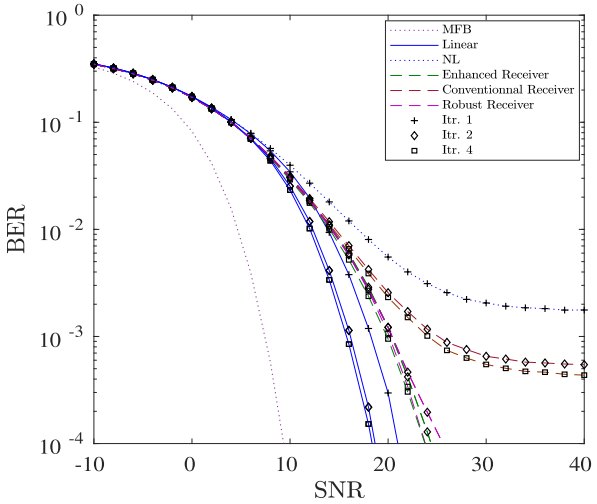

FIGURE 7. BER of high power signal from the low power user considering enhanced DC-NOMA-IB-DFE, robust and conventional receivers with IBO = 7 dB and β= 9 dB.

Fig. 7 and Fig. 8 show the BER performance for the Enhanced DC-NOMA-IB-DFE receiver associated to the high power and low power signals, respectively, from the perspective of the low power user. Clearly, in both cases the performance improves significantly with the number of iterations, outperforming significantly the Robust and Conventional receivers. We note that this improvement is more significant for the detection of the low power signal compared with high power signal. This can be explained by the fact that the nonlinear distortion estimation is mainly conditioned by the high-power signal. In this case, and as is observed in Fig. 7, the performance results of the proposed receiver are close to the ones of the Robust receiver. This means that the Robust receiver will consider the distortion like IUI and reduce it after each iteration. However, in Fig. 8, we show that the gaps between the Robust and the Enhanced DC-NOMA-IB-DFE can still be relevant in term of BER performance, which means that the residual distortion is not negligible and cannot be treated as IUI. Therefore, unlike the Robust receiver, the proposed receiver, takes into account the nonlinear degradation and cancel it before the detection of the low power signal.

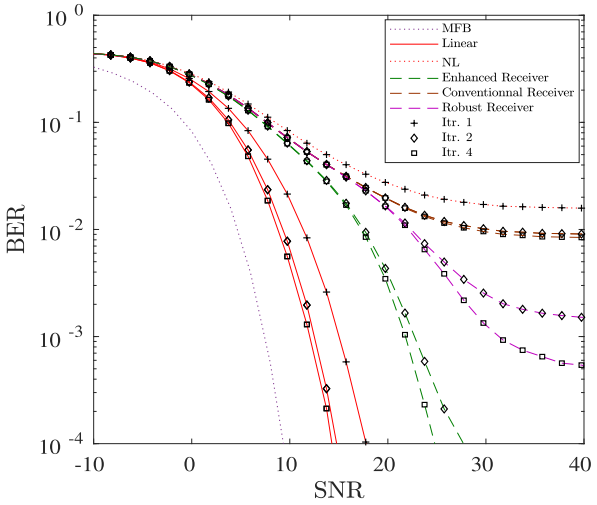

FIGURE 8. BER of low power signal from the low power user considering enhanced DC-NOMA-IB-DFE, robust and conventional receivers with IBO = 7 dB and β= 9 dB.

To confirm the efficiency of our receiver, Fig. 9 and Fig. 10 present a comparison between the Enhanced DC-NOMA-IB-DFE, Robust NOMA-IB-DFE receivers and predistortion scheme, cited in [38], with different MLP configurations: (a) In this scenario the MLP neural network is configured with two inputs, two outputs and one hidden layer with three neurons. (b) the NN is composed of two inputs, six neurons in the hidden layer and two linear neurons in the output layer. Firstly, for low IBO value, we can confirm from these figures that the proposed compensation scheme is able to improve the system performance for low and high power signals and that it is very close to that of the predistortion scheme with a simple configuration of neurons (a). On other hand, although the predistortion scheme (b) characterized by large number of neurons in hidden layer, can outperform slightly the Enhanced DC NOMA-IB-DFE receiver, its complexity can be too high for practical implementations.

Let us now access the impact of the modulation order on the proposed nonlinear distortion cancellation schemes. Fig. 11 shows the BER of the Enhanced DC-NOMA-IB-DFE receiver after the fourth iteration, considering 16-QAM modulation and IBO = 7 dB. From these plots, it can be

[3]This work can easily be extended to other constellations by following the IB-DFE design for general constellations of [9].

TABLE 1. Aprroximate number of operations required for the predistortion NOMA-IB-DFE and enhanced DC NOMA-IB-DFE receiver for $I_{max} = 3$.

	Computational complexity	$N = 256$	$N = 512$
predistortion NOMA-IB-DFE	$2 \times I_{\max} \times \mathcal{O}(NN^{'}\ [\vartheta\iota + \iota\kappa + \kappa])$	43008	86016
NOMA-DC-IB-DFE	$2 \times I_{\max} \times \mathcal{O}(NN^{'} \log NN^{'})$	18496	40690
Complexity gain		0,57	0,52

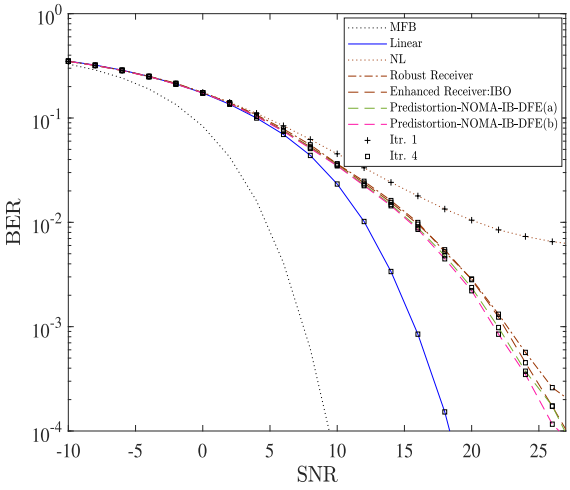

FIGURE 9. BER of high power signal from the low power user considering the enhanced DC-NOMA-IB-DFE, robust NOMA-IB-DFE receivers and predistortion schemes with different neurons configurations with IBO = 5 dB.

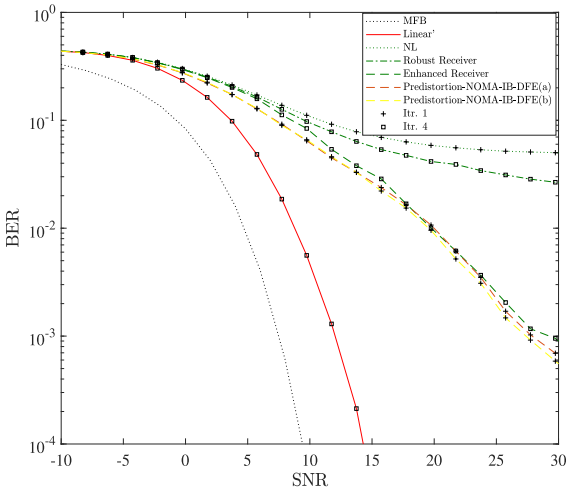

FIGURE 10. BER of low power signal from the low power user considering the enhanced DC-NOMA-IB-DFE, robust NOMA-IB-DFE receivers and predistortion schemes with different neurons configurations with IBO = 5 dB.

confirmed that, although the low power user is considerably affected by the nonlinear degradation caused by the RF impairment, our proposed receiver is able to compensate the distortion effects after four iterations, reducing substantially the error floors. Indeed, for large constellations the iterative receivers are even more useful, since those constellations suffer more from interference.

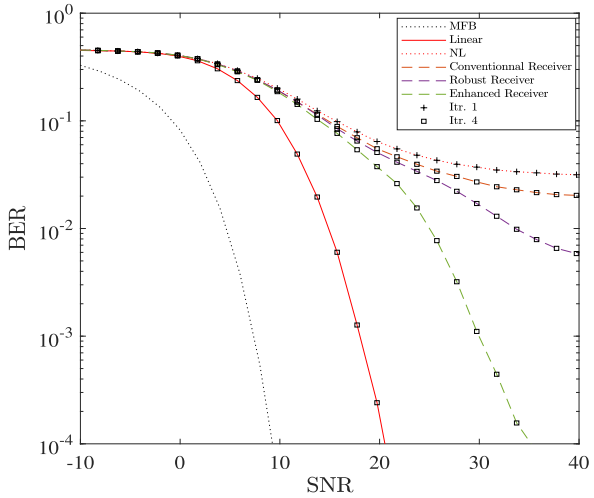

FIGURE 11. BER of low power signal from the low power user considering the enhanced DC-NOMA-IB-DFE and robust NOMA-IB-DFE receivers with IBO = 7 dB and 16-QAM modulation.

In order to see the impact of number of users on the Enhanced DC-NOMA-IB-DFE performance, Fig. 12, shows the BER performance of the proposed receiver in presence of nonlinear polynomial model with IBO = 7 dB and three active users configurations, where the first user represents the high power user and the third one is the low power user. The power separation ratios between the users referred to $\beta_{k,k+1}$. From this figure we can confirm that although the power amplifier component inhibit considerably the performance, especially for the low power user, a significant improvement is obtained when using the Enhanced DC-NOMA-IB-DFE receiver after four iterations. Moreover, we can observe that the BER behaviors saturate to a deterministic value limiting its performance for different users. This can be explained by the sensitivity of SC systems regarding the nonlinearities due to their large envelope fluctuations.

Fig. 13 and Fig. 14 show the BER performance associated to both high power and low power signals, from the perspective of the low power user, in presence of nonlinear polynomial model. We consider different values of IBOs and a receiver that makes a iterative cancellation of the nonlinear distortion. We can observe from these figures that the NOMA systems with iterative compensation scheme outperform the Robust NOMA-IB-DFE receiver and can be inherently sturdy to the different nonlinear distortions levels. However, we can clearly notice that the performance gains associated to the detection of low and high power signals decrease for low IBO values. Indeed, the difference between the ideal case and

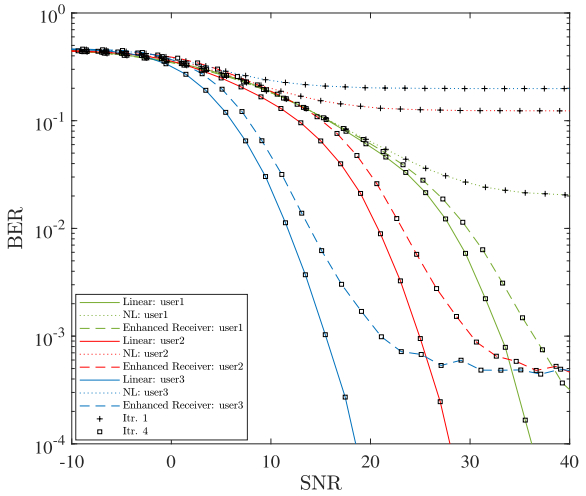

FIGURE 12. BER considering the enhanced DC-NOMA-IB-DFE receiver for $K = 3$, with β_{12}= 7 dB, β_{23}= 5 dB and different IBO values.

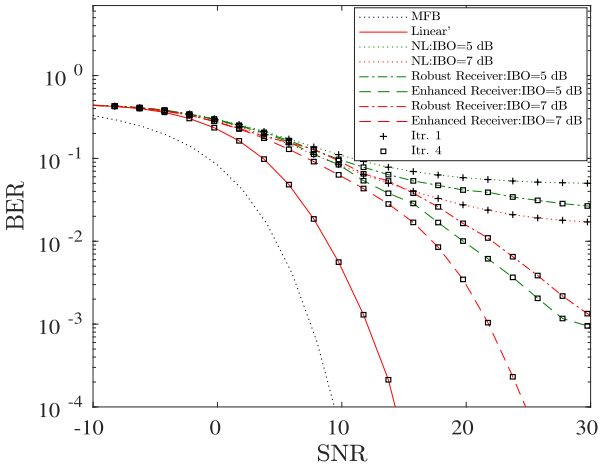

FIGURE 14. BER of low power signal from the low power user considering the enhanced DC-NOMA-IB-DFE and robust NOMA-IB-DFE receivers with β= 12 dB and different IBO values.

the BER after the fourth iteration of the proposed algorithm is not negligible when IBO = 5 dB for all cases. However, a significant improvement is obtained when IBO = 7 dB with the same number of iterations.

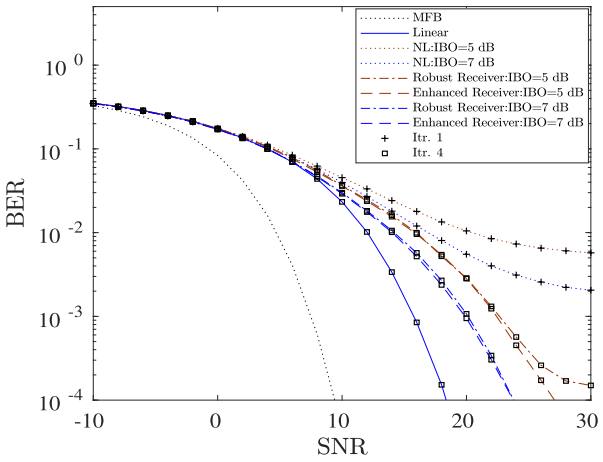

FIGURE 13. BER of high power signal from the low power user considering the enhanced DC-NOMA-IB-DFE and robust NOMA-IB-DFE receivers with β= 12 dB and different IBO values.

Let us now access the impact of β on the NOMA-SC with IB-DFE receivers performance. Fig. 15 and Fig. 16 present the BER associated to both high power and low power signals, from the perspective of the low power user, for different values of β and a nonlinearity with IBO = 7 dB. From the two figures, it can be observed that when β = 9 dB we are able to obtain accurate estimates of the nonlinear distortion term. In fact, by estimating the nonlinear distortion from the high power signal and after four iterations, we can have considerable performance gains relative to the Robust NOMA-IB-FDE receiver associated to the detection of both signals (i.e., low power and high power signals). However, with $\beta = 6$ dB, the performance is far from the one obtained by a linear transmission in both detection scenarios. Moreover, the performance of Enhanced DC-NOMA-IB-DFE and Robust NOMA-IB-DFE are very close, especially for the detection of the low power signal. This effect is due to the poor performance of the detection of the high power signal (i.e., it has a high error floor), since it was detected by assuming that the low power signal is a noisy term. Consequently, a high error floor can be occurred when estimating the distortion noise. This means that $\beta = 6$ dB is not enough to separate the two signals and to estimate perfectly the nonlinear effects.

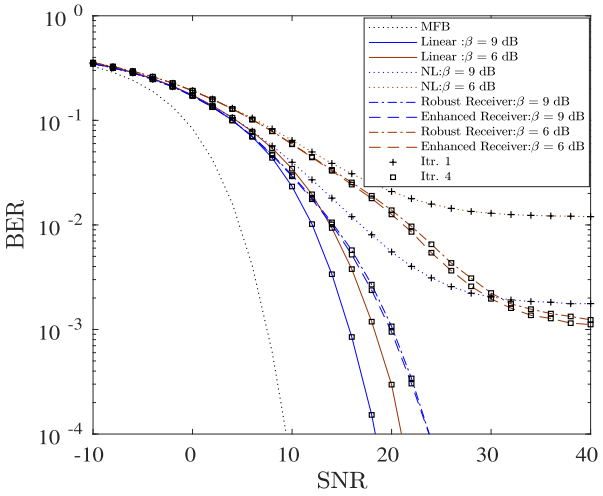

FIGURE 15. BER of high power signal from the low power user considering the enhanced DC-NOMA-IB-DFE and robust NOMA-IB-DFE receivers with IBO = 7 dB and different values of β.

To study the robustness of the proposed receiver, we consider a scenario with imperfect CSI information. In [39] authors modeled the channel gain estimation for each pth subcarrier as a function of the true response channel plus a

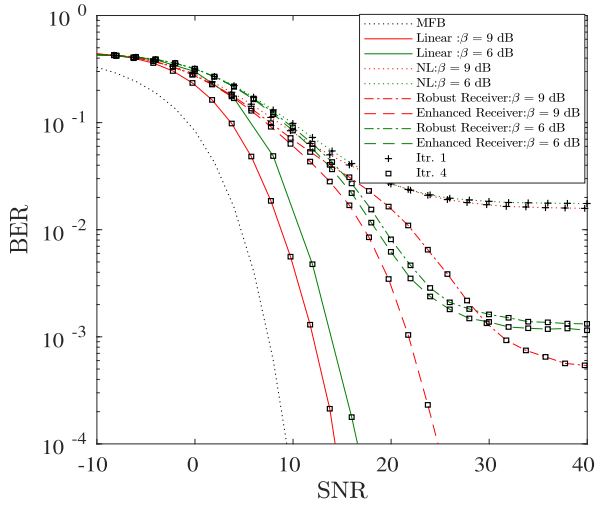

FIGURE 16. BER of low power signal from the low power user considering the enhanced DC-IB-FDE and robust NOMA-IB-DFE receivers with IBO = 7 dB and different values of β.

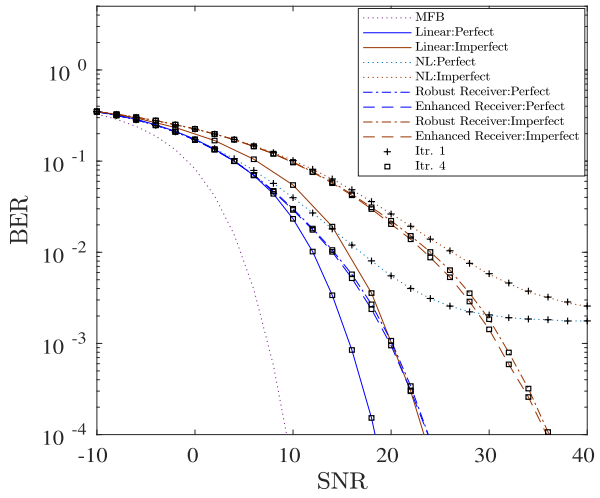

FIGURE 17. BER of high power signal from the low power user considering enhanced NOMA DC-IB-FDE and robust NOMA IB-DFE receivers with β= 9 dB and IBO = 7 dB under perfect and imperfect CSI.

error component,[4] i.e.,

$$\hat{H}_p^{(k)} = H_p^{(k)} + E_p^{(k)} \tag{37}$$

where $\left\{E_p^{(k)} : 0 \le p \le NN' - 1\right\} \in \mathbb{C}^{NN'}$ is a complex Gaussian distributed with power $2\sigma_E^2$.

Fig. 17 and Fig. 18 show the BER performance of the high power and low power signals from the low power user detection, respectively, employing Robust NOMA-IB-DFE and Enhanced NOMA-DC-IB-DFE receivers with different iterations (i.e., Itr= $\{1, 4\}$). From the two figures, it can be noted that our proposed design outperform the Robust NOMA-IB-DFE even with imperfect CSI. Regarding the detection of the high power and low power signals,

[4]the generalization to other channel estimation error models is straightforward

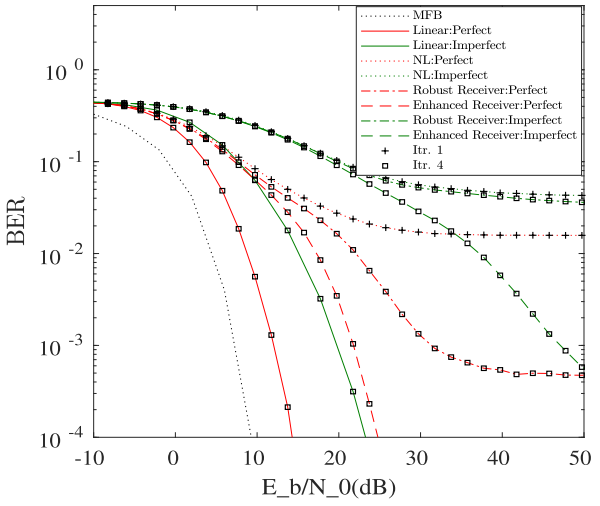

FIGURE 18. BER of low power signal from the low power user considering enhanced NOMA DC-IB-FDE and robust NOMA IB-DFE receivers with β= 9 dB and IBO = 7 dB under perfect and imperfect CSI.

when using NOMA-DC-IB-DFE receiver, we observe that having imperfect CSI leads to some performance degradation relatively to the case with perfect CSI. However, even with imperfect CSI, the BER of Enhanced DC-NOMA-IB-DFE receiver still improves with the iterations. Therefore, our main conclusions are also valid with imperfect CSI. We note that, although the proposed receiver is able to compensate the effect of nonlinear degradation, reducing the effects of ISI and IUI when detecting the low power signal, the gains are smaller when we have channel estimation errors, even after 4 iterations. This loss is explained by two factors: (i) the channel estimation errors affect considerably the detection of the high power signal; (ii) since the estimation of the distortions terms depend essentially from the high power signal, when β is high, a high error floor can affect the cancellation process when using the proposed receiver.

VII. CONCLUSION

In this work, we considered SC-FDE signals combined with NOMA schemes in the downlink transmission impaired by a generalized memoryless polynomial HPA. A detailed evaluation of nonlinear SC-FDE-NOMA transmission techniques was carried out, involving theoretical computations of PSD. A set of performance results was presented and discussed. The obtained PSD of the residual inter user interference and distortion components corresponding to the low power user is important since the nonlinear distortion depends mainly on the high-power signals. To reduce the effect of RF impairment and cancel the interference caused by different users, an efficient detection is achieved using iterative receivers with joint multiuser and distortion cancellation. The proposed Enhanced DC-NOMA-IB-DFE receiver can provide significant improvement in the reduction of the in-band distortion allowing then better energy efficiency. In addition, it was showed that even with strong nonlinear

distortions effects, and imperfect CSI we can be able to obtain acceptable performances especially for high β values.

It should be pointed out that the practical implementation of Enhanced DC NOMA-IB-DFE is more-or-less straightforward. The only additional requirement when compared with conventional receivers is the knowledge of the nonlinear characteristics, which is not difficult to achieve, since the nonlinear parameters change much slowly than other channel parameters. As with other NOMA techniques, it might involve security challenges, since a given user might detect the signals intended to other users, but this can easily be overcome by employing standard scrambling techniques or other security measures.

REFERENCES

[1] L. Dai, B. Wang, Y. Yuan, S. Han, I. Chih-Lin, and Z. Wang, "Non-orthogonal multiple access for 5G: Solutions, challenges, opportunities, and future research trends," *IEEE Commun. Mag.*, vol. 53, no. 9, pp. 74–81, Sep. 2015.

[2] S. Zhang, X. Xu, L. Lu, Y. Wu, G. He, and Y. Chen, "Sparse code multiple access: An energy efficient uplink approach for 5G wireless systems," in *Proc. IEEE Global Commun. Conf.*, Dec. 2014, pp. 4782–4787.

[3] S. M. R. Islam, N. Avazov, O. A. Dobre, and K.-S. Kwak, "Power-domain non-orthogonal multiple access (NOMA) in 5G systems: Potentials and challenges," *IEEE Commun. Surveys Tuts.*, vol. 19, no. 2, pp. 721–742, 2nd Quart., 2017.

[4] M. Wildemeersch, T. Q. S. Quek, M. Kountouris, A. Rabbachin, and C. H. Slump, "Successive interference cancellation in heterogeneous networks," *IEEE Trans. Commun.*, vol. 62, no. 12, pp. 4440–4453, Dec. 2014.

[5] L. Cimini, "Analysis and simulation of a digital mobile channel using orthogonal frequency division multiplexing," *IEEE Trans. Commun.*, vol. C-33, no. 7, pp. 665–675, Jul. 1985.

[6] H. Sari, G. Karam, and I. Jeanclaude, "An analysis of orthogonal frequency-division multiplexing for mobile radio applications," in *Proc. IEEE Veh. Technol. Conf. (VTC)*, Mar. 1994, pp. 1635–1639.

[7] M. Tuchler, R. Koetter, and A. C. Singer, "Turbo equalization: Principles and new results," *IEEE Trans. Commun.*, vol. 50, no. 5, pp. 754–767, May 2002.

[8] N. Benvenuto and S. Tomasin, "Block iterative DFE for single carrier modulation," *Electron. Lett.*, vol. 38, no. 19, pp. 1144–1145, 2002.

[9] R. Dinis, P. Montezuma, and J. Silva, "Iterative frequency domain equalization for general constellations," in *Proc. IEEE Sarnoff Symp.*, Apr. 2010, pp. 1–5.

[10] N. Benvenuto and S. Tomasin, "Iterative design and detection of a DFE in the frequency domain," *IEEE Trans. Commun.*, vol. 53, no. 11, pp. 1867–1875, Nov. 2005.

[11] R. Dinis, R. Kalbasi, D. Falconer, and A. H. Banihashemi, "Iterative layered space-time receivers for single-carrier transmission over severe time-dispersive channels," *IEEE Commun. Lett.*, vol. 8, no. 9, pp. 579–581, Sep. 2004.

[12] J. Silva, R. Dinis, P. Montezuma, and N. Souto, "Single-carrier frequency domain equalisation with hierarchical constellations: An efficient transmission technique for broadcast and multicast systems," *IET Commun.*, vol. 6, no. 13, pp. 2065–2073, Sep. 2012.

[13] M. Bayraktar and G. M. Guvensen, "Adaptation of code-domain NOMA to SC-FDE based overloaded mmWave hybrid massive MIMO," *IEEE Commun. Lett.*, vol. 26, no. 3, pp. 667–671, Mar. 2022.

[14] J. Goto, O. Nakamura, K. Yokomakura, Y. Hamaguchi, S. Ibi, and S. Sampei, "A frequency domain scheduling for uplink single carrier non-orthogonal multiple access with iterative interference cancellation," in *Proc. IEEE Veh. Technol. Conf.*, Sep. 2014, pp. 1–5.

[15] F. Liu and M. Petrova, "Proportional fair scheduling for downlink single-carrier NOMA systems," in *Proc. IEEE Global Commun. Conf.*, Dec. 2017, pp. 1–7.

[16] Z. Mokhtari and R. Dinis, "Sum-rate of cell free massive MIMO systems with power amplifier non-linearity," *IEEE Access*, vol. 9, pp. 141927–141937, 2021.

[17] J. Qi and S. Aissa, "Analysis and compensation of I/Q imbalance in MIMO transmit-receive diversity systems," *IEEE Trans. Commun.*, vol. 58, no. 5, pp. 1546–1556, May 2010.

[18] E. Björnson, J. Hoydis, and L. Sanguinetti, "Massive MIMO networks: Spectral, energy, and hardware efficiency," *Found. Trends Signal Process.*, vol. 11, nos. 3–4, pp. 154–655, 2017.

[19] J. Guerreiro, R. Dinis, and P. Montezuma, "Analytical performance evaluation of precoding techniques for nonlinear massive MIMO systems with channel estimation errors," *IEEE Trans. Commun.*, vol. 66, no. 4, pp. 1440–1451, Apr. 2018.

[20] F. Gregorio, S. Werner, T. I. Laakso, and J. Cousseau, "Receiver cancellation technique for nonlinear power amplifier distortion in SDMA–OFDM systems," *IEEE Trans. Veh. Technol.*, vol. 56, no. 5, pp. 2499–2516, Sep. 2007.

[21] D. Dardari, V. Tralli, and A. Vaccari, "A theoretical characterization of nonlinear distortion effects in OFDM systems," *IEEE Trans. Commun.*, vol. 48, no. 10, pp. 1755–1764, Oct. 2000.

[22] O. B. H. Belkacem, M. L. Ammari, and R. Dinis, "Performance analysis of NOMA in 5G systems with HPA nonlinearities," *IEEE Access*, vol. 8, pp. 158327–158334, 2020.

[23] T. Lee and H. Ochiai, "Characterization of power spectral density for nonlinearly amplified OFDM signals based on cross-correlation coefficient," *EURASIP J. Wireless Commun. Netw.*, vol. 2014, no. 1, pp. 1–15, Dec. 2014.

[24] J. Brown, "On a cross-correlation property for stationary random processes," *IEEE Trans. Inf. Theory*, vol. IT-3, no. 1, pp. 28–31, Mar. 1957.

[25] W. A. Gardner, "Exploitation of spectral redundancy in cyclostationary signals," *IEEE Signal Process. Mag.*, vol. 8, no. 2, pp. 14–36, Apr. 1991.

[26] C. Tellambura, "A coding technique for reducing peak-to-average power ratio in OFDM," in *Proc. IEEE GLOBECOM*, vol. 4, Nov. 1998, pp. 2783–2787.

[27] H. Ochiai, "Performance analysis of peak power and band-limited OFDM system with linear scaling," *IEEE Trans. Wireless Commun.*, vol. 2, no. 5, pp. 1055–1065, Sep. 2003.

[28] R. Raich, H. Qian, and G. T. Zhou, "Orthogonal polynomials for power amplifier modeling and predistorter design," *IEEE Trans. Veh. Technol.*, vol. 53, no. 5, pp. 1468–1479, Sep. 2004.

[29] O. B. H. Belkacem, R. Dinis, and M. L. Ammari, "Nonlinear effects in NOMA-OFDM systems: Analytical signal characterization and receiver design," *IEEE Trans. Veh. Technol.*, vol. 72, no. 3, pp. 3739–3750, Mar. 2023.

[30] J. Guerreiro, R. Dinis, P. Montezuma, and M. M. da Silva, "Nonlinear effects in NOMA signals: Performance evaluation and receiver design," in *Proc. IEEE Veh. Technol. Conf.*, Sep. 2019, pp. 1–5.

[31] A. Kaye, D. George, and M. Eric, "Analysis and compensation of bandpass nonlinearities for communications," *IEEE Trans. Commun.*, vol. C-20, no. 5, pp. 965–972, Oct. 1972.

[32] P. N. Landin and D. Rönnow, "RF PA modeling considering odd-even and odd order polynomials," in *Proc. IEEE Symp. Commun. Veh. Technol. Benelux (SCVT)*, Nov. 2015, pp. 1–6.

[33] S. P. A. Papoulis, *Probability, Random Variables and Stochastic Processes*. Stochastic Proc, 2002.

[34] R. Dinis and A. Gusmao, "A class of nonlinear signal processing schemes for bandwidth-efficient OFDM transmission with low envelope fluctuation," *IEEE Trans. Commun.*, vol. 52, no. 11, pp. 2009–2018, Nov. 2004.

[35] J. Guerreiro, R. Dinis, and P. Montezuma, "Low-complexity SC-FDE techniques for massive MIMO schemes with low-resolution ADCs," *IEEE Trans. Commun.*, vol. 67, no. 3, pp. 2368–2380, Mar. 2019.

[36] L. Lv, H. Jiang, Z. Ding, Q. Ye, N. Al-Dhahir, and J. Chen, "Secure non-orthogonal multiple access: An interference engineering perspective," *IEEE Netw.*, vol. 35, no. 4, pp. 278–285, Jul. 2021.

[37] F. C. Ribeiro, J. Guerreiro, R. Dinis, F. Cercas, and D. N. K. Jayakody, "Multi-user detection for the downlink of NOMA systems with multi-antenna schemes and power-efficient amplifiers," *Phys. Commun.*, vol. 33, pp. 199–205, Apr. 2019.

[38] R. Zayani, H. Shaïek, and D. Roviras, "Ping-pong joint optimization of PAPR reduction and HPA linearization in OFDM systems," *IEEE Trans. Broadcast.*, vol. 65, no. 2, pp. 308–315, Jun. 2019.

[39] E. K. S. Au and W. H. Mow, "Effect of non-linearity on the performance of a MIMO zero-forcing receiver with channel estimation errors," in *Proc. IEEE Int. Conf. Commun.*, Jun. 2007, pp. 4150–4155.

OUSSAMA BEN HAJ BELKACEM (Member, IEEE) received the Engineering and M.Sc. degrees in telecommunications from the University of Sousse, Tunisia, in 2007 and 2009, respectively, and the Ph.D. degree in telecommunications from the National Engineering School of Tunis (ENIT), Tunisia, in 2015. Since 2010, he has been a Research Associate with the Innovation of Communicant and Cooperative Mobiles Laboratory (Innov'Com), Higher School of Communications of Tunis, University of Carthage. From 2012 to 2015, he was with the Department of Telecommunication and Networking, High Institute of Computer Science (ISI), Tunis, Tunisia, as a contractual Assistant Professor. Since 2015, he has been an Assistant Professor with the High Institute of Computer Science Mahdia, University of Monastir, Tunisia. His research interests include MIMO technologies, NOMA, orthogonal frequency-division multiplexing systems, high power amplifier nonlinearity, PAPR reduction, energy harvesting, neural network compensation, space time coding, and equalization and performance analysis.

RUI DINIS (Senior Member, IEEE) received the Ph.D. degree from Instituto Superior Técnico (IST), Technical University of Lisbon, Portugal, in 2001, and the Habilitation degree in telecommunications from Faculdade de Ciências e Tecnologia (FCT), Universidade Nova de Lisboa (UNL), in 2010. From 2001 to 2008, he was a Professor with IST. He was a Researcher with Centro de Análise e Processamento de Sinal (CAPS), IST, from 1992 to 2005, and a Researcher with Instituto de Sistemas e Robótica (ISR), from 2005 to 2008. In 2003, he was an Invited Professor with Carleton University, Ottawa, ON, Canada. Since 2009, he has been a Researcher with Instituto de Telecomunicações (IT). He is currently an Associate Professor with FCT–UNL. He has been actively involved in several national and international research projects in the broadband wireless communications area. His research interests include transmission, estimation, and detection techniques. He is an IEEE VTS Distinguished Speaker and an IEEE ComSoc Distinguished Lecturer. He is or was an Editor of IEEE TRANSACTIONS ON WIRELESS COMMUNICATIONS, IEEE TRANSACTIONS ON COMMUNICATIONS, IEEE TRANSACTIONS ON VEHICULAR TECHNOLOGY, IEEE OPEN JOURNAL OF THE COMMUNICATIONS SOCIETY, and *Physical Communication* (Elsevier). He was the Guest Editor of the *Physical Communication* (Elsevier) Special Issue on Broadband Single-Carrier Transmission Techniques.

MOHAMED LASSAAD AMMARI (Member, IEEE) received the Engineering degree from the University of Carthage, Tunis, Tunisia, in 1995, and the M.Sc. and Ph.D. degrees from Université Laval, Québec City, QC, Canada, in 2000 and 2003, respectively. From 2003 to 2005, he was a Research Associate with the Laboratory of Communications and Integrated Microelectronics, École de Technologie Supérieure, Montreal, QC, Canada. He is currently a Professor with the National Engineering School of Sousse, Sousse, Tunisia. He is also an Active Team Member with the Networked Objects, Control, and Communication Systems (NOCCS), National Engineering School of Sousse, University of Sousse, Sousse. His research interests include channel equalization, multiple-input–multiple-output orthogonal frequency-division multiplexing systems, turbo detection, space-time coding, and adaptive modulation.